

Absolute Magnitude Calibration for Red Giants based on the Colour – Magnitude Diagrams of Galactic Clusters. I- Calibration with V and $B-V$

S. Karaali^{†,A,B}, S. Bilir^A, and E. Yaz Gökçe^A

^A Istanbul University, Faculty of Sciences, Department of Astronomy and Space Sciences, 34119, Istanbul, Turkey

^B Email: karsa@istanbul.edu.tr

Abstract: We present an absolute magnitude calibration for red giants with the colour magnitude diagrams of six Galactic clusters with different metallicities i.e. M92, M13, M5, 47 Tuc, M67, and NGC 6791. The combination of the absolute magnitude offset from the fiducial of giant sequence of the cluster M5 with the corresponding metallicity offset provides calibration for absolute magnitude estimation for red giants for a given $(B - V)_0$ colour. The calibration is defined in the colour interval $0.75 \leq (B - V)_0 \leq 1.50$ mag and it covers the metallicity interval $-2.15 < [Fe/H] \leq +0.37$ dex. 91% of the absolute magnitude residuals obtained by the application of the procedure to another set of Galactic clusters lie in the interval $-0.40 < \Delta M \leq +0.40$ mag. The mean and the standard deviation of the residuals are 0.05 and 0.19 mag, respectively. We fitted the absolute magnitude also to metallicity and age for a limited sub-sample of $(B - V)_0$ colour, just to test the effect of age in absolute magnitude calibration. Comparison of the mean and the standard deviation of the residuals evaluated by this procedure with the corresponding ones provided by the procedure where the absolute magnitude fitted to a third degree polynomial of metallicity show that the age parameter may be omitted in absolute magnitude estimation of red giants. The derived relations are applicable to stars older than 4 Gyr, the age of the youngest calibrating cluster.

Keywords: stars: distances - (stars:) giants - (Galaxy:) globular clusters: individual (M92, M13, M5, 47 Tuc) - (Galaxy:) open clusters: individual (M67, NGC 6791)

Introduction

Stellar kinematics and metallicity are two primary means to deduce the history of our Galaxy. However, such goals can not be achieved without stellar distances. The distance to a star can be evaluated by trigonometric or photometric parallaxes. Trigonometric parallaxes are only available for nearby stars where *Hipparcos* (ESA 1997) is the main supplier for the data. For stars at large distances, the use of photometric parallaxes is unavoidable. In other words the study of the Galactic structure is strictly tied to precise determination of absolute magnitudes.

Different methods can be used for absolute magnitude determination where most of them are devoted to dwarfs. The method used in the Strömgren's $uvby - \beta$ (Nissen & Schuster 1991) and in the UBV (Laird, Carney & Latham 1988) photometries depends on the absolute magnitude offset from a standard main-sequence. In recent years the derivation of absolute magnitudes has been carried out by means of colour-

absolute magnitude diagrams of some specific clusters whose metal abundances are generally adopted as the mean metal abundance for a Galactic population, such as thin, thick discs and halo. The studies of Phleps et al. (2000) and Chen et al. (2001) can be given as examples. A slightly different approach is that of Siegel et al. (2002) where two relations, one for stars with solar-like abundances and another one for metal-poor stars were derived between M_R and the colour index $R - I$, where M_R is the absolute magnitude in the R filter of Johnson system. For a star of given metallicity and colour, absolute magnitude can be estimated by *linear* interpolation of *two* ridgelines and by means of *linear* extrapolation beyond the metal-poor ridgeline.

The most recent procedure used for absolute magnitude determination consists of finding the most likely values of the stellar parameters, given the measured atmospheric ones, and the time spent by a star in each region of the H-R diagram. In practice, researchers select the subset of isochrones with $[M/H] \pm \Delta_{[M/H]}$, where $\Delta_{[M/H]}$ is the estimated error on the metallicity, for each set of derived T_{eff} , $\log g$ and $[M/H]$. Then a Gaussian weight is associated to each point of the selected isochrones, which depends on the measured atmospheric parameters and the considered errors. This criterion

[†] Retired.

allows the algorithm to select only the points whose values are closed by the pipeline. For details of this procedure we cite the works of Breddels et al. (2010) and Zwitter et al. (2010). This procedure is based on many parameters. Hence it provides absolute magnitudes with high accuracy. Also it can be applied to both dwarf and giant stars simultaneously.

In Karaali et al. (2003), we presented a procedure for the photometric parallax estimation of dwarf stars which depends on the absolute magnitude offset from the main-sequence of the Hyades cluster. In this study, we will use a similar procedure for the absolute magnitude estimation of red giants by using the apparent magnitude-colour diagrams of Galactic clusters with different metallicities. In Section 2 we present the data. The procedure used for calibration is given in Section 3, and Section 4 is devoted to summary and discussion.

2 Data

Six clusters with different metallicities, i.e. M92, M13, M5, 47 Tuc, M67, and NGC 6791, were selected for our program. The range of the metallicity given in iron abundance is $-2.15 \leq [Fe/H] \leq +0.37$ dex. The $V - M_V$ apparent distance modulus, $(V - M_V)_0$ true distance modulus, $E(B - V)$ colour excess, and $[Fe/H]$ iron abundance are given in Table 1, whereas the V and $B - V$ data are presented in Table 2. We adopted $R = A_V/E(B - V) = 3.1$ to convert between colour excess and extinction. Although different numerical values appeared in the literature for specific regions of our Galaxy, a single value is applicable everywhere. Different distance moduli and interstellar extinctions were cited in the literature for the clusters. The data in Table 1 and Table 2 are taken from the authors cited in the reference list of Table 1. The V and $B - V$ data of M92 were taken from two sources, i.e. Sandage (1970) and Stetson & Harris (1988), and combined to obtain a colour magnitude diagram with largest range in $B - V$. Data used in the combination of the final colour-magnitude diagram are shown with bold face in Table 2. The distance modulus, reddening, and metallicity for this cluster were taken from Gratton et al. (1997). All the data for each cluster M5, M67 and NGC6791 were taken from a single source, as indicated in Table 1. Whereas, we refer two references for the clusters M13 and 47 Tuc. The V and $B - V$ data were taken from the first reference, but the second one refers to their $V - M_V$ distance modulus, $E(B - V)$ colour-excess and $[Fe/H]$ metallicity. The reason of this selection is to obtain the best fitting of the colour magnitude diagrams to the isochrones (see section 3). Thus, in the case of more than one reference in Table1, the last one refers to the distance modulus, colour excess, and metallicity. The original V and $B - V$ data refer to the fiducial sequence, i.e. giants, sub-

Table 1: Data for the clusters used in our work.

Cluster	$V - M_V$ (mag)	$E(B - V)$ (mag)	$(V - M_V)_0$ (mag)	$[Fe/H]$ (dex)	$[\alpha/Fe]$	Reference
M92	14.80	0.025	14.72	-2.15	0.33	(1),(2),(3)
M13	14.44	0.020	14.38	-1.41	0.22	(1),(3)
M5	14.50	0.020	14.44	-1.17	0.24	(4)
47 Tuc	13.37	0.040	13.25	-0.80	0.27	(5),(6)
M67	9.65	0.038	9.53	-0.04	—	(7)
NGC6791	13.25	0.100	12.94	0.37	—	(7)

(1) Sandage (1970), (2) Stetson & Harris (1988), (3) Gratton et al. (1997), (4) Sandquist et al. (1996), (5) Hesser et al. (1987), (6) Percival et al. (2002), (7) Sandage, Lubin & Vandenberg (2003)

giants, and main-sequence stars of the clusters. We plotted these sequences on a diagram for each cluster and identified red giants by means of their positions in the diagram. The $(V, B - V)$ points in Table 2 consist of the fiducial sequence of the referred cluster. Hence, they represent the cluster in question quite well. However, they are not error free. The errors for these couples may be a bit larger for the photographic magnitude and colours of the clusters M92 and M13 than the CCD ones of the other clusters. As noted above the bright magnitudes and the corresponding colours of the cluster M92, and all magnitude and colours of the cluster M13 which were taken from Sandage (1970) are photographic data. We will see in Section 3 that the data of these clusters are in good agreement with the data of the other clusters investigated by using CCD technic. We, then fitted the fiducial sequence of the red giants to a sixth degree polynomial for all clusters, except M92 for which a seventh degree polynomial was necessary for a good correlation coefficient. The calibration of V_0 is as follows:

Table 3: Numerical values of the coefficients a_i ($i = 0, 1, 2, 3, 4, 5, 6, 7$) in Eq. (1).

Cluster	M92	M13	M5	47 Tuc	M67	NGC 6791
$(B - V)_0$ interval	[0.55, 1.38]	[0.83, 1.60]	[0.66, 1.63]	[0.75, 1.66]	[0.86, 1.52]	[1.04, 1.44]
a_7	1260.209	—	—	—	—	—
a_6	-8985.514	98.924	6.240	143.690	-1353.155	-12852.318
a_5	27088.160	-753.362	-76.946	-1101.784	9923.884	97469.551
a_4	-44677.194	2376.106	332.511	3484.807	-30101.159	-307314.819
a_3	43443.029	-3970.848	-700.971	-5820.763	48311.495	515575.766
a_2	-24830.833	3710.911	789.927	5421.810	-43245.725	-485363.694
a_1	7688.065	-1845.252	-465.120	-2679.997	20450.384	243057.102
a_0	-972.939	396.915	128.221	565.960	-3974.116	-50554.897

$$V_0 = \sum_{i=1}^7 a_i (B - V)_0^i \quad (1)$$

The numerical values of the coefficients a_i ($i = 0, 1, 2, 3, 4, 5, 6, 7$) are given in Table 3, and the corresponding diagrams are presented in Fig. 1. The $(B - V)_0$ -interval in the first line of the table indicate to the range of $(B - V)_0$ available for each cluster.

Table 2: Fiducial red giant sequences for six Galactic clusters used for calibration. The data of M92 are taken from two different sources and combined to obtain a diagram with largest $(B - V)$ -interval. The colours and magnitudes used for the calibration are given with bold face. 10 and 12 fiducial points of M67 and NGC 6791, respectively, in the original catalogues which correspond to sub-giants/main-sequence stars have not been considered in our work.

$B - V$	V	$(B - V)_0$	V_0	$B - V$	V	$(B - V)_0$	V_0	$B - V$	V	$(B - V)_0$	V_0	$B - V$	V	$(B - V)_0$	V_0
M92 (Stetson & Harris 1988)				M92 (Sandage 1970)				M5 (cont.)				M67 (cont.)			
0.690	15.80	0.665	15.72	1.400	11.90	1.375	11.82	1.023	13.91	1.003	13.85	0.937	12.86	0.899	12.74
0.677	16.00	0.652	15.92	1.300	12.09	1.275	12.01	1.003	14.09	0.983	14.03	0.900	13.05	0.862	12.93
0.664	16.20	0.639	16.12	1.200	12.39	1.175	12.31	0.965	14.30	0.945	14.24	0.850	13.05	—	—
0.652	16.40	0.627	16.32	1.100	12.75	1.075	12.67	0.903	14.70	0.883	14.64	0.800	12.90	—	—
0.639	16.60	0.614	16.52	1.000	13.15	0.975	13.07	0.867	14.94	0.847	14.87	0.750	12.75	—	—
0.627	16.80	0.602	16.72	0.900	13.58	0.875	13.50	0.855	15.09	0.835	15.03	0.700	12.63	—	—
0.615	17.00	0.590	16.92	0.800	14.11	0.775	14.03	0.831	15.32	0.811	15.26	0.650	12.61	—	—
0.603	17.20	0.578	17.12	0.750	14.45	0.725	14.37	0.814	15.50	0.794	15.44	0.600	12.60	—	—
0.591	17.40	0.566	17.32	0.700	15.05	0.675	14.97	0.798	15.70	0.778	15.63	0.535	12.85	—	—
0.578	17.60	0.553	17.52	M92 (Combined Sequence)				0.783	15.89	0.763	15.83	0.578	13.15	—	—
0.552	17.80	0.527	17.72	—	—	1.375	11.82	0.773	16.10	0.753	16.04	0.559	13.50	—	—
0.500	17.96	0.475	17.88	—	—	1.275	12.01	0.756	16.30	0.736	16.24	0.562	13.75	—	—
0.476	18.00	0.451	17.92	—	—	1.175	12.31	0.746	16.48	0.726	16.42	NGC 6791			
0.450	18.08	0.425	18.00	—	—	1.075	12.67	0.731	16.70	0.711	16.63	1.535	14.25	1.435	13.94
0.419	18.20	0.394	18.12	—	—	0.975	13.07	0.724	16.92	0.704	16.86	1.500	14.45	1.400	14.14
0.400	18.32	0.375	18.24	—	—	0.875	13.50	0.711	17.10	0.691	17.04	1.450	14.73	1.350	14.42
0.396	18.40	0.371	18.32	—	—	0.775	14.03	0.714	17.10	0.694	17.04	1.400	15.04	1.300	14.73
0.388	18.60	0.363	18.52	—	—	0.614	16.52	0.717	17.30	0.697	17.24	1.331	15.50	1.231	15.19
0.390	18.80	0.365	18.72	—	—	0.602	16.72	0.694	17.50	0.674	17.44	1.274	16.00	1.174	15.69
0.397	19.00	0.372	18.92	—	—	0.590	16.92	0.684	17.65	0.664	17.59	1.228	16.50	1.128	16.19
0.406	19.20	0.381	19.12	—	—	0.578	17.12	47 Tuc				1.191	17.00	1.091	16.69
0.418	19.40	0.393	19.32	—	—	0.566	17.32	1.70	11.70	1.66	11.58	1.175	17.25	1.075	16.94
0.434	19.60	0.409	19.52	—	—	0.553	17.52	1.60	11.85	1.56	11.73	1.140	17.50	1.040	17.19
0.454	19.80	0.429	19.72	M13				1.50	12.03	1.46	11.91	1.100	17.50	—	—
0.477	20.00	0.452	19.92	1.62	12.05	1.60	11.99	1.40	12.23	1.36	12.11	1.050	17.46	—	—
0.502	20.20	0.477	20.12	1.50	12.05	1.48	11.99	1.30	12.55	1.26	12.43	1.000	17.39	—	—
0.529	20.40	0.504	20.32	1.40	12.16	1.38	12.10	1.19	13.00	1.15	12.88	0.950	17.35	—	—
0.559	20.60	0.534	20.52	1.30	12.40	1.28	12.34	1.10	13.50	1.06	13.38	0.900	17.42	—	—
0.594	20.80	0.569	20.72	1.20	12.70	1.18	12.64	1.01	14.00	0.97	13.88	0.888	17.50	—	—
0.632	21.00	0.607	20.92	1.10	13.09	1.08	13.03	0.95	14.50	0.91	14.38	0.875	17.75	—	—
0.675	21.20	0.650	21.12	1.00	13.55	0.98	13.49	0.90	15.00	0.86	14.88	0.888	18.00	—	—
0.718	21.40	0.693	21.32	0.95	13.85	0.93	13.79	0.83	16.00	0.79	15.88	0.909	18.25	—	—
0.763	21.60	0.738	21.52	0.90	14.15	0.88	14.09	0.81	16.50	0.77	16.38	0.942	18.50	—	—
0.810	21.80	0.785	21.72	0.85	14.64	0.83	14.58	0.79	17.00	0.75	16.88	0.974	18.75	—	—
0.855	22.00	0.830	21.92	M5				M67				1.010	19.00	—	—
0.901	22.20	0.876	22.12	1.653	12.06	1.633	11.99	1.555	9.00	1.517	8.88	—	—	—	—
0.949	22.40	0.924	22.32	1.582	12.17	1.562	12.11	1.430	9.50	1.392	9.38	—	—	—	—
0.996	22.60	0.971	22.52	1.483	12.30	1.463	12.24	1.320	10.00	1.282	9.88	—	—	—	—
1.042	22.80	1.017	22.72	1.416	12.46	1.396	12.39	1.220	10.50	1.182	10.38	—	—	—	—
1.074	23.00	1.049	22.92	1.342	12.63	1.322	12.57	1.127	11.00	1.089	10.88	—	—	—	—
1.089	23.20	1.064	23.12	1.253	12.90	1.233	12.84	1.059	11.50	1.021	11.38	—	—	—	—
1.092	23.40	1.067	23.32	1.194	13.10	1.174	13.04	1.032	11.75	0.994	11.63	—	—	—	—
1.086	23.60	1.061	23.52	1.141	13.32	1.121	13.26	1.000	12.18	0.962	12.06	—	—	—	—
1.077	23.80	1.052	23.72	1.092	13.52	1.072	13.46	0.974	12.50	0.936	12.38	—	—	—	—
1.060	24.00	1.035	23.92	1.053	13.72	1.033	13.66	0.950	12.72	0.912	12.60	—	—	—	—

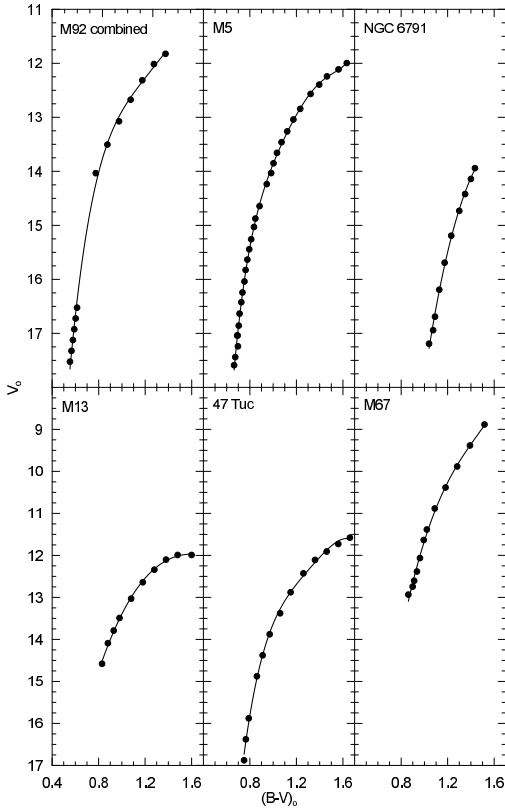


Figure 1: $V_0 \times (B - V)_0$ colour-apparent magnitude diagrams for six Galactic clusters used for the absolute magnitude calibration.

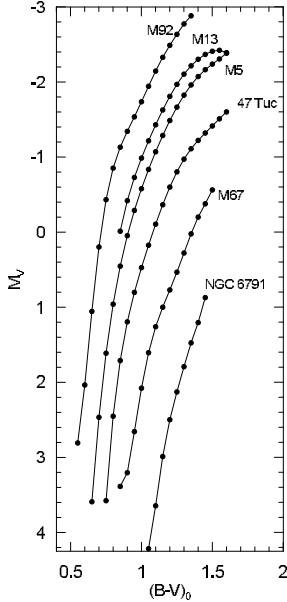


Figure 2: $M_V \times (B - V)_0$ colour-absolute magnitude diagrams for six Galactic clusters used for the absolute magnitude calibration.

3 The Procedure

3.1 Absolute Magnitude Offset as a Function of Metallicity Offset

The procedure consists of calibration of the absolute magnitude offsets from the fiducial giant sequence of a standard cluster as a function of metallicity offsets. For this purpose we proceeded as in the following. We estimated the absolute magnitudes for the $(B - V)_0$ colours given in Table 4 for the cluster sample by combining the V_0 apparent magnitudes evaluated by Eq. (1) and the true distance modulus (μ_0) of the cluster in question, i.e.

$$M_V = V_0 - \mu_0. \quad (2)$$

Then, we plotted the absolute magnitudes versus $(B - V)_0$ colours. Fig. 2 shows that the absolute magnitude is colour and metallicity dependent. It increases (algebraically) with increasing metallicity and decreasing colour. We fitted the $M_V - (B - V)_0$ diagrams to isochrones in order to test our data and the procedure. The diagrams of five clusters with metallicity $[Fe/H] \leq 0.2$ dex could be fitted to the Padova isochrones (Marigo et al. 2008). Whereas it could not be carried out for the cluster NGC 6791 whose metallicity is beyond the upper metallicity limit of the Padova isochrones, i.e. $[Fe/H] = 0.2$ dex. Hence, we used the isochrones of the Victoria-Regina Stellar Models (VandenBerg, Bergbusch & Dowler 2006) for the cluster NGC 6791. The results are given in Fig. 3. There is a good fitting of the fiducial sequence of the red giants to the isochrones for a large interval of the $(B - V)_0$ colour index. However, one can notice a deviation for the metal-poor clusters at the red segment. We should note that the fitting presented in Fig. 3, for each cluster, is the best one of different combinations of distance modulus, reddening, and metallicity. We adopted the sequence of M5 as the standard one and we evaluated the ΔM offsets from the fiducial giant sequence of M5 (Table 4). Now, we can replace ΔM versus the corresponding $\Delta[Fe/H]$ iron abundance residuals and obtain the required calibration. This is carried out for the colours $(B - V)_0 = 0.75, 1.00, 1.25$, and 1.50 mag just to test of the procedure, and the results are given in Table 5 and Fig. 4. This procedure can be applied to any $(B - V)_0$ colour-interval for which the sample clusters are defined.

We adopted this interval in our study as $0.75 \leq (B - V)_0 \leq 1.50$ mag where at least three clusters are defined, and we evaluated ΔM offsets for each colour. Then, we combined them with the corresponding $\Delta[Fe/H]$ residuals and obtained the final calibrations. The general form of the equation for the calibrations is as follows:

$$\Delta M = b_0 + b_1 X + b_2 X^2 + b_3 X^3 \quad (3)$$

Table 4: M_V absolute magnitudes and ΔM offsets estimated for a set of $(B - V)_0$ interval for six Galactic clusters used in the calibration.

	M92		M13		M5		47 Tuc		M67		NGC 6791	
$(B - V)_0$	M_V	ΔM	M_V	ΔM	M_V	ΔM	M_V	ΔM	M_V	ΔM	M_V	ΔM
0.55	2.81	—	—	—	—	—	—	—	—	—	—	—
0.60	2.04	—	—	—	—	—	—	—	—	—	—	—
0.65	1.06	-2.54	—	—	3.59	0	—	—	—	—	—	—
0.70	0.20	-2.27	—	—	2.47	0	—	—	—	—	—	—
0.75	-0.43	-2.05	—	—	1.61	0	3.58	1.96	—	—	—	—
0.80	-0.85	-1.81	—	—	0.96	0	2.45	1.49	—	—	—	—
0.85	-1.13	-1.58	-0.01	-0.47	0.45	0	1.71	1.26	3.39	2.93	—	—
0.90	-1.34	-1.39	-0.42	-0.47	0.05	0	1.19	1.15	3.20	3.16	—	—
0.95	-1.54	-1.25	-0.73	-0.44	-0.29	0	0.80	1.09	2.66	2.95	—	—
1.00	-1.74	-1.16	-0.99	-0.41	-0.58	0	0.47	1.05	2.08	2.66	—	—
1.05	-1.94	-1.11	-1.22	-0.38	-0.84	0	0.17	1.01	1.61	2.44	4.22	5.05
1.10	-2.15	-1.08	-1.43	-0.36	-1.07	0	-0.11	0.96	1.26	2.33	3.64	4.72
1.15	-2.33	-1.04	-1.63	-0.34	-1.29	0	-0.37	0.92	1.00	2.29	2.99	4.28
1.20	-2.49	-1.00	-1.81	-0.32	-1.49	0	-0.60	0.89	0.77	2.26	2.50	3.98
1.25	-2.64	-0.97	-1.97	-0.30	-1.67	0	-0.80	0.86	0.53	2.20	2.13	3.79
1.30	-2.77	-0.95	-2.11	-0.28	-1.83	0	-0.97	0.85	0.28	2.10	1.79	3.62
1.35	-2.88	-0.92	-2.22	-0.26	-1.96	0	-1.11	0.85	0.02	1.98	1.47	3.44
1.40	—	—	-2.30	-0.23	-2.07	0	-1.22	0.85	-0.20	1.87	1.20	3.28
1.45	—	—	-2.37	-0.20	-2.16	0	-1.32	0.84	-0.38	1.79	0.87	3.04
1.50	—	—	-2.41	-0.17	-2.24	0	-1.42	0.82	-0.56	1.68	—	—
1.55	—	—	-2.42	-0.12	-2.31	0	-1.51	0.80	—	—	—	—
1.60	—	—	-2.39	-0.01	-2.38	0	-1.60	0.78	—	—	—	—

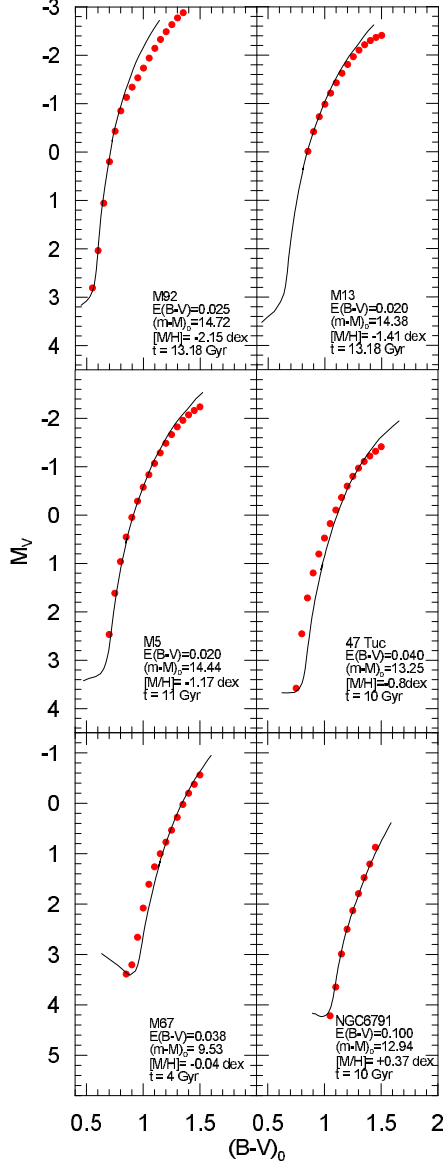


Figure 3: $M_V \times (B-V)_0$ absolute magnitude-colour diagrams fitted to isochrones.

Table 5: ΔM and $\Delta[Fe/H]$ offsets for four $(B-V)_0$ intervals.

$(B-V)_0$	$\Delta[Fe/H]$	ΔM
0.75	-0.98	-2.05
	0.00	0.00
	0.37	1.96
1.00	-0.98	-1.16
	-0.24	-0.41
	0.00	0.00
	0.37	1.05
	1.13	2.66
1.25	-0.98	-0.97
	-0.24	-0.30
	0.00	0.00
	0.37	0.86
	1.13	2.20
1.50	1.54	3.79
	-0.24	-0.17
	0.00	0.00
	0.37	0.82
	1.13	1.68

where $X = \Delta[Fe/H]$.

ΔM could be fitted in terms of $\Delta[Fe/H]$ for the colours $0.75 \leq (B-V)_0 \leq 0.82$ mag by a quadratic polynomial, whereas a cubic polynomial provided higher correlation for $(B-V)_0 \geq 0.83$ mag. The absolute magnitudes estimated via Eq. (2) for 76 colours and the corresponding b_i ($i = 0, 1, 2, 3$) coefficients are given in Table 6. However, the numerical values for ΔM are omitted and the diagrams for the calibrations are not displayed for avoiding space consuming. One can use any data set taken from Table 6 depending on the required accuracy, and apply it to stars whose iron abundances are available.

The calibration of ΔM in terms of $\Delta[Fe/H]$ is carried out for the colour interval $0.75 \leq (B-V)_0 \leq 1.50$ mag in steps of 0.1 mag. Small step is necessary to isolate an observational error on $B-V$ plus a wrong error due to reddening. The origin of the mentioned errors is the trend of the Red Giant Branch (RGB) sequence. As it is very steep, a small error in $B-V$ implies a large change in the absolute magnitude.

Iron abundance, $[Fe/H]$, is not the only parameter determining the chemistry of the star but also alpha enhancement, $[\alpha/Fe]$, is surely important. The $[\alpha/Fe]$ values for seven clusters used in our work are given in Table 1 (and Table 10, see Section 3.3). One can notice an inverse-correlation between two sets of abundances, i.e. $[\alpha/Fe]$ increases with decreasing

$[Fe/H]$. Hence, we do not expect any considerable change in the numerical value of ΔM in the case of addition of an alpha enhancement term in Eq. (3).

3.2 Absolute Magnitude as a Function of Metallicity and Age

Age plays an important role in the trend of the fiducial sequence of the RGB. Hence, we added age as a parameter in the calibration of the absolute magnitude as follows:

$$M_V = c_0 + c_1x + c_2y + c_3x^2 + c_4y^2 + c_5xy \quad (4)$$

where x and y indicate the metallicity and age, i.e. $x = [Fe/H]$ and $y = t$. The metallicities and ages of the clusters can be used and the coefficients c_i ($i = 0, 1, 2, 3, 4, 5$) can be determined. The common domain of the clusters is $1.05 \leq (B - V)_0 \leq 1.35$ mag. Hence, this procedure works only for the $(B - V)_0$ colour interval just cited. However, we could extend this procedure to the interval $0.85 \leq (B - V)_0 < 1.05$ mag. by a small modification of Eq. (4) as in the following:

$$M_V = d_0 + d_1x + d_2y + d_3x^2 + d_4xy \quad (5)$$

Thus, we omitted the fifth term in Eq. (4) and obtained Eq. (5) with five coefficients, i.e. d_i ($i = 0, 1, 2, 3, 4$), which can be determined by using the metallicities and ages of the clusters M92, M13, M5, 47 Tuc, and M67. The elimination of the fifth term is due to fact that its coefficient (c_4) is the (absolutely) smallest one (see Section 3.3). One can use Eq. (4) and Eq. (5) simultaneously and estimate the absolute magnitudes of red giants with $0.85 \leq (B - V)_0 < 1.35$.

We used the metallicities of the clusters M92, M13, M5, 47 Tuc, M67, and NGC 6791 in Table 1, their ages in Table 7 and the absolute magnitudes of these clusters in Table 4 for $(B - V)_0 = 1.05, 1.10, 1.15, 1.20, 1.25, 1.30, 1.35$, and determined seven sets of coefficients c_i ($i = 0, 1, 2, 3, 4, 5$). The coefficients d_i ($i = 0, 1, 2, 3, 4$) were determined by the same procedure for the same $(B - V)_0$ colour-indices omitting the data of NGC 6791, however. The results are given in Table 8 and Table 9. The aim of the limitation for the $(B - V)_0$ colour is to test the effect of age on absolute magnitude estimation. One can extend the determination of the coefficients c_i and d_i to a larger $(B - V)_0$ interval, accordingly.

Table 7: Ages of the clusters. The ages of the clusters used for the absolute magnitude calibration, M92, M13, M5, 47 Tuc, M67 and NGC 6791 are determined in this study as showed Fig. 3. Whereas, the ages of the clusters used for the application of the procedure are taken from the authors given in the reference list.

Cluster	t (Gyr)	Cluster	t (Gyr)	Ref.
M92	13.18	M3	12.1	1
M13	13.18	M53	13.2	2
M5	11.00	M71	10.1	1
47 Tuc	10.00	NGC 188	5.9	3
M67	4.00	NGC 6366	8.0	1
NGC 6791	10.00	IC 4499	11.2	1
—	—	Ter 7	8.9	1

(1) Salaris & Weiss (2002), (2) Santos & Piatti (2004), (3) Meibom et al. (2009)

Table 8: Numerical values of the coefficients in Eq. (4) for seven $(B - V)_0$ colour indices.

$(B - V)_0$	c_0	c_1	c_2	c_3	c_4	c_5
1.05	-3.62	12.00	1.88	-0.08	-0.12	-0.86
1.10	-3.73	11.48	1.80	-0.13	-0.12	-0.83
1.15	-3.95	11.54	1.80	-0.28	-0.12	-0.88
1.20	-4.14	11.58	1.79	-0.37	-0.12	-0.91
1.25	-4.51	12.19	1.84	-0.54	-0.13	-0.99
1.30	-5.04	12.26	1.94	-0.56	-0.13	-1.01
1.35	-5.7	12.84	2.09	-0.69	-0.14	-1.09

3.3 Application of the Method

3.3.1 Absolute Magnitudes Estimated by means of Metallicity

We applied the method to seven clusters with different metallicities, i.e. M3, M53, M71, NGC 188, NGC 6366, IC 4499, and Ter 7, as explained in the following. The reason of choosing clusters instead of individual field giants is that clusters provide absolute magnitudes for comparison with the ones estimated by means of our method. The distance modulus, colour excess and metallicity of the clusters are given in Table 10, whereas the V and $B - V$ data are presented in Table 11 and they are calibrated in Fig. 5. The data in Table 10 and Table 11 are taken from the authors cited in the reference list of Table 10. In the case of two references, the first one refers to the V , $(B - V)$ fiducial sequence, whereas the second one refers to the data given in the same table.

As in the case of Table 2, the $(V, B - V)$ points in Table 11 consist of the fiducial sequence of the referred cluster. Hence, they represent the cluster in question quite well. However, they are not error free. Although one can expect a bit larger error for the photographic data of the cluster M3, this did not

Table 6: M_V absolute magnitudes estimated for six Galactic clusters and the numerical values of b_i ($i = 0, 1, 2, 3$) coefficients in Eq. (3). The last column gives the range of the metallicity $[Fe/H]$ (dex) for the star whose absolute magnitude would be estimated. R^2 is the square of the correlation coefficient.

	M92	M13	M5	47 Tuc	M67	NGC6791							
$(B - V)_0$	M_V	M_V	M_V	M_V	M_V	M_V	b_0	b_1	b_2	b_3	R^2	$[Fe/H]$ -interval	
0.75	-0.43	—	1.61	3.58	—	—	0.0000	4.4252	2.3862	—	1	[-2.15, -0.80]	
0.76	-0.53	—	1.47	3.31	—	—	0.0000	4.1750	2.1787	—	1	[-2.15, -0.80]	
0.77	-0.62	—	1.33	3.07	—	—	0.0000	3.9541	2.0013	—	1	[-2.15, -0.80]	
0.78	-0.71	—	1.20	2.84	—	—	0.0000	3.7585	1.8506	—	1	[-2.15, -0.80]	
0.79	-0.78	—	1.08	2.64	—	—	0.0000	3.5884	1.7260	—	1	[-2.15, -0.80]	
0.80	-0.85	—	0.96	2.45	—	—	0.0000	3.4340	1.6174	—	1	[-2.15, -0.80]	
0.81	-0.92	—	0.85	2.28	—	—	0.0000	3.2995	1.5280	—	1	[-2.15, -0.80]	
0.82	-0.98	—	0.74	2.12	—	—	0.0000	3.1841	1.4602	—	1	[-2.15, -0.80]	
0.83	-1.03	0.19	0.64	1.97	—	—	0.0000	2.3726	2.5943	1.9544	1	[-2.15, -0.80]	
0.84	-1.08	0.09	0.54	1.84	—	—	0.0000	2.3826	2.3782	1.6756	1	[-2.15, -0.80]	
0.85	-1.13	-0.01	0.45	1.71	3.39	—	0.1142	2.8836	0.4740	-0.7204	0.9982	[-2.15, -0.04]	
0.86	-1.18	-0.11	0.36	1.59	3.40	—	0.1012	2.8215	0.5387	-0.6475	0.9987	[-2.15, -0.04]	
0.87	-1.22	-0.19	0.28	1.48	3.39	—	0.0912	2.7659	0.5891	-0.5928	0.9989	[-2.15, -0.04]	
0.88	-1.26	-0.27	0.20	1.38	3.35	—	0.0837	2.7200	0.6255	-0.5570	0.9991	[-2.15, -0.04]	
0.89	-1.30	-0.35	0.12	1.29	3.28	—	0.0777	2.6791	0.6510	-0.5338	0.9992	[-2.15, -0.04]	
0.90	-1.34	-0.42	0.05	1.19	3.20	—	0.0738	2.6431	0.6668	-0.5212	0.9993	[-2.15, -0.04]	
0.91	-1.38	-0.49	-0.03	1.11	3.11	—	0.0714	2.6111	0.6750	-0.5170	0.9993	[-2.15, -0.04]	
0.92	-1.42	-0.55	-0.10	1.03	3.00	—	0.0700	2.5811	0.6764	-0.5187	0.9993	[-2.15, -0.04]	
0.93	-1.46	-0.61	-0.16	0.95	2.89	—	0.0694	2.5559	0.6727	-0.5266	0.9993	[-2.15, -0.04]	
0.94	-1.50	-0.67	-0.23	0.87	2.78	—	0.0700	2.5339	0.6654	-0.5392	0.9993	[-2.15, -0.04]	
0.95	-1.54	-0.73	-0.29	0.80	2.66	—	0.0711	2.5108	0.6542	-0.5509	0.9992	[-2.15, -0.04]	
0.96	-1.58	-0.78	-0.35	0.73	2.54	—	0.0721	2.4897	0.6408	-0.5640	0.9992	[-2.15, -0.04]	
0.97	-1.62	-0.84	-0.41	0.66	2.42	—	0.0730	2.4687	0.6264	-0.5771	0.9991	[-2.15, -0.04]	
0.98	-1.66	-0.89	-0.47	0.60	2.30	—	0.0750	2.4500	0.6108	-0.5907	0.9990	[-2.15, -0.04]	
0.99	-1.70	-0.94	-0.52	0.54	2.19	—	0.0763	2.4308	0.5947	-0.6018	0.9990	[-2.15, -0.04]	
1.00	-1.74	-0.99	-0.58	0.47	2.08	—	0.0776	2.4115	0.5787	-0.6115	0.9989	[-2.15, -0.04]	
1.01	-1.78	-1.03	-0.63	0.41	1.97	—	0.0792	2.3902	0.5631	-0.6175	0.9988	[-2.15, -0.04]	
1.02	-1.82	-1.08	-0.69	0.35	1.87	—	0.0797	2.3698	0.5483	-0.6214	0.9987	[-2.15, -0.04]	
1.03	-1.86	-1.13	-0.74	0.29	1.78	—	0.0811	2.3512	0.5351	-0.6258	0.9987	[-2.15, -0.04]	
1.04	-1.90	-1.17	-0.79	0.23	1.69	4.25	0.0793	1.2145	0.4534	0.5178	0.9878	[-2.15, +0.37]	
1.05	-1.94	-1.22	-0.84	0.17	1.61	4.22	0.0792	1.1656	0.4407	0.5486	0.9872	[-2.15, +0.37]	
1.06	-1.99	-1.26	-0.89	0.12	1.53	4.14	0.0793	1.1393	0.4306	0.5586	0.9969	[-2.15, +0.37]	
1.07	-2.03	-1.30	-0.93	0.06	1.45	4.04	0.0797	1.1289	0.4226	0.5536	0.9869	[-2.15, +0.37]	
1.08	-2.07	-1.35	-0.98	0.00	1.38	3.92	0.0798	1.1318	0.4169	0.5363	0.9871	[-2.15, +0.37]	
1.09	-2.11	-1.39	-1.03	-0.05	1.32	3.78	0.0790	1.1456	0.4138	0.5099	0.9875	[-2.15, +0.37]	
1.10	-2.15	-1.43	-1.07	-0.11	1.26	3.64	0.0783	1.1630	0.4114	0.4802	0.9880	[-2.15, +0.37]	
1.11	-2.18	-1.47	-1.12	-0.16	1.20	3.50	0.0780	1.1862	0.4111	0.4460	0.9886	[-2.15, +0.37]	
1.12	-2.22	-1.51	-1.16	-0.21	1.15	3.37	0.0775	1.2102	0.4112	0.4119	0.9893	[-2.15, +0.37]	
1.13	-2.26	-1.55	-1.20	-0.27	1.10	3.23	0.0764	1.2342	0.4128	0.3779	0.9899	[-2.15, +0.37]	
1.14	-2.29	-1.59	-1.25	-0.32	1.05	3.11	0.0760	1.2573	0.4144	0.3455	0.9906	[-2.15, +0.37]	
1.15	-2.33	-1.63	-1.29	-0.37	1.00	2.99	0.0756	1.2792	0.4168	0.3151	0.9912	[-2.15, +0.37]	
1.16	-2.36	-1.67	-1.33	-0.42	0.95	2.88	0.0745	1.2978	0.4191	0.2876	0.9918	[-2.15, +0.37]	
1.17	-2.40	-1.70	-1.37	-0.46	0.91	2.77	0.0736	1.3134	0.4211	0.2635	0.9923	[-2.15, +0.37]	
1.18	-2.43	-1.74	-1.41	-0.51	0.86	2.67	0.0734	1.3258	0.4230	0.2422	0.9927	[-2.15, +0.37]	
1.19	-2.46	-1.78	-1.45	-0.56	0.82	2.58	0.0730	1.3367	0.4252	0.2229	0.9931	[-2.15, +0.37]	
1.20	-2.49	-1.81	-1.49	-0.60	0.77	2.50	0.0734	1.3423	0.4263	0.2078	0.9934	[-2.15, +0.37]	
1.21	-2.52	-1.84	-1.52	-0.64	0.72	2.42	0.0731	1.3463	0.4263	0.1950	0.9937	[-2.15, +0.37]	
1.22	-2.55	-1.88	-1.56	-0.69	0.68	2.34	0.0735	1.3483	0.4256	0.1844	0.9939	[-2.15, +0.37]	
1.23	-2.58	-1.91	-1.60	-0.73	0.63	2.27	0.0739	1.3469	0.4236	0.1761	0.9940	[-2.15, +0.37]	
1.24	-2.61	-1.94	-1.63	-0.77	0.58	2.20	0.0747	1.3444	0.4205	0.1695	0.9941	[-2.15, +0.37]	
1.25	-2.64	-1.97	-1.67	-0.80	0.53	2.13	0.0755	1.3394	0.4165	0.1646	0.9941	[-2.15, +0.37]	
1.26	-2.66	-2.00	-1.70	-0.84	0.48	2.06	0.0770	1.3328	0.4114	0.1611	0.9941	[-2.15, +0.37]	
1.27	-2.69	-2.03	-1.73	-0.88	0.43	1.99	0.0784	1.3274	0.4053	0.1575	0.9940	[-2.15, +0.37]	
1.28	-2.72	-2.05	-1.76	-0.91	0.38	1.92	0.0796	1.3179	0.3975	0.1564	0.9939	[-2.15, +0.37]	
1.29	-2.75	-2.08	-1.80	-0.94	0.33	1.86	0.0818	1.3102	0.3889	0.1548	0.9937	[-2.15, +0.37]	
1.30	-2.77	-2.11	-1.83	-0.97	0.28	1.79	0.0840	1.3004	0.3794	0.1545	0.9935	[-2.15, +0.37]	
1.31	-2.80	-2.13	-1.85	-1.00	0.23	1.73	0.0862	1.2898	0.3701	0.1542	0.9933	[-2.15, +0.37]	
1.32	-2.82	-2.15	-1.88	-1.03	0.17	1.66	0.0881	1.2792	0.3604	0.1542	0.9930	[-2.15, +0.37]	
1.33	-2.85	-2.18	-1.91	-1.06	0.12	1.60	0.0906	1.2670	0.3507	0.1546	0.9927	[-2.15, +0.37]	
1.34	-2.87	-2.20	-1.94	-1.09	0.07	1.53	0.0934	1.2547	0.3425	0.1546	0.9923	[-2.15, +0.37]	
1.35	-2.88	-2.22	-1.96	-1.11	0.02	1.47	0.0957	1.2417	0.3355	0.1542	0.9919	[-2.15, +0.37]	
1.36	-2.89	-2.24	-1.99	-1.14	-0.03	1.42	0.0975	1.2280	0.3312	0.1527	0.9915	[-2.15, +0.37]	
1.37	-2.90	-2.25	-2.01	-1.16	-0.07	1.36	0.1002	1.2118	0.3297	0.1510	0.9910	[-2.15, +0.37]	
1.38	-2.90	-2.27	-2.03	-1.18	-0.12	1.31	0.1018	1.1942	0.3321	0.1473	0.9905	[-2.15, +0.37]	
1.39	—	-2.29	-2.05	-1.20	-0.16	1.26	0.1766	1.7354	-1.0652	0.8117	0.9931	[-1.41, +0.37]	
1.40	—	-2.30	-2.07	-1.22	-0.20	1.20	0.1794	1.7251	-1.0742	0.8125	0.9927	[-1.41, +0.37]	
1.41	—	-2.32	-2.09	-1.24	-0.24	1.15	0.1814	1.7150	-1.0787	0.8103	0.9924	[-1.41, +0.37]	
1.42	—	-2.33	-2.11	-1.26	-0.28	1.10	0.1829	1.7047	-1.0739	0.8010	0.9921	[-1.41, +0.37]	
1.43	—	-2.35	-2.13	-1.28	-0.31	1.03	0.1837	1.6942	-1.0561	0.7812	0.9918	[-1.41, +0.37]	
1.44	—	-2.36	-2.15	-1.30	-0.35	0.96	0.1833	1.6817	-1.0186	0.7470	0.9915	[-1.41, +0.37]	
1.45	—	-2.37	-2.16	-1.32	-0.38	—	0.0000	1.6233	2.6509	-2.3794	1	[-1.41, -0.04]	
1.46	—	-2.38	-2.18	-1.34	-0.41	—	0.0000	1.6073	2.6821	-2.4063	1	[-1.41, -0.04]	
1.47	—	-2.39	-2.20	-1.36	-0.45	—	0.0000	1.5920	2.7009	-2.4241	1	[-1.41, -0.04]	
1.48	—	-2.40	-2.21	-1.38	-0.48	—	0.0000	1.5742	2.7399	-2.4585	1	[-1.41, -0.04]	
1.49	—	-2.40	-2.23	-1.40	-0.52	—	0.0000	1.5530	2.7816	-2.4954	1	[-1.41, -0.04]	
1.50	—	-2.41	-2.24	-1.42	-0.56	—	0.0000	1.5327	2.8113	-2.527	1	[-1.41, -0.04]	

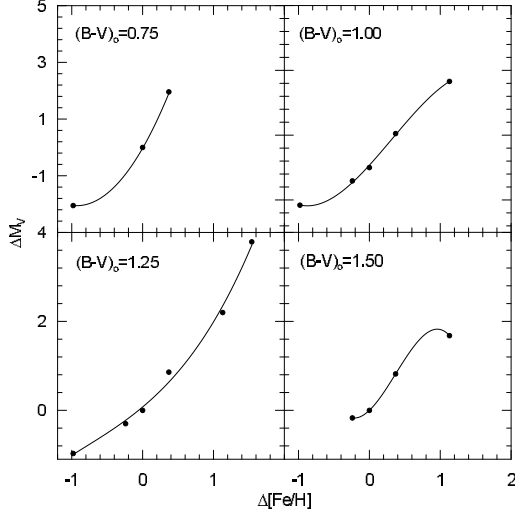


Figure 4: Calibration of the absolute magnitude offsets (ΔM) as a function of metallicity offsets ($\Delta[Fe/H]$) for four colour-indices.

Table 9: Numerical values of the coefficients in Eq. (5) for seven $(B - V)_0$ colour indices.

$(B - V)_0$	d_0	d_1	d_2	d_3	d_4
1.05	0.13	4.18	0.42	1.82	0.25
1.10	-0.13	3.96	0.39	1.69	0.23
1.15	-0.27	3.86	0.36	1.59	0.21
1.20	-0.42	3.80	0.34	1.52	0.19
1.25	-0.65	3.77	0.34	1.49	0.18
1.30	-0.96	3.75	0.35	1.51	0.19
1.35	-1.32	3.69	0.38	1.53	0.20

Table 10: Data for the clusters used for the application of the method.

Cluster	$V - M_V$ (mag)	$E(B - V)$ (mag)	$(V - M_V)_0$ (mag)	$[Fe/H]$ (dex)	$[\alpha/Fe]$ (dex)	Reference
M3	15.07	0.010	15.04	-1.50	0.29	(1),(2)
M53	16.32	0.020	16.26	-1.99	—	(3),(2)
M71	13.70	0.280	12.83	-0.78	0.39	(4)
NGC188	11.40	0.095	11.11	-0.01	—	(5)
NGC6366	—	0.700	12.26	-0.67	—	(6)
IC4499	17.08	0.230	16.37	-1.53	—	(7),(2)
Ter7	17.01	0.070	16.79	-0.87	0.009	(8)

(1) Sandage (1970), (2) Harris (1996, 2010), (3) Rey et al. (1998), (4) Hodder et al. (1992), (5) Meibom et al. (2009), (6) Alonso et al. (1997), (7) Sarajedini (1993), (8) Buonanno et al. (1995)

show up (see Table 12, column 7).

We evaluated the ΔM absolute magnitude offsets by using the Eq. (3) for the $(B - V)_0$ -domain of each cluster, added them to the corresponding absolute magnitude of the cluster M5 and obtained the absolute magnitude $(M_V)_*$. The results are presented in Table 12. The columns give: (1) $(B - V)_0$ colour index, (2) M_V , absolute magnitude for the cluster estimated by its colour magnitude diagram, (3) $(M_V)_{M5}$, absolute magnitude corresponding to the cluster M5, (4) $\Delta[Fe/H]$, metallicity offset from the metallicity of the cluster M5, (5) ΔM , absolute magnitude offset from the fiducial giant sequence of the cluster M5, (6) $(M_V)_*$, the absolute magnitude estimated by the procedure, (7) absolute magnitude residuals: $M_V - (M_V)_*$. The cluster name is indicated at the top of the corresponding columns.

The differences between the absolute magnitudes estimated in this study and the ones evaluated via the colour magnitude diagrams of the clusters, i.e. $M_V - (M_V)_*$, lie between -0.61 and $+0.66$ mag. However, the range of 91% of the residuals is shorter, i.e. $-0.4 \leq M_V - (M_V)_* \leq +0.4$ mag, and their mean and standard deviation are only 0.05 and 0.19 mag, respectively. The positive large values correspond to the data of cluster NGC 188, whereas the negative ones originate from the data of cluster NGC 6366. The results are given in Table 13 and Fig. 6.

3.3.2 Absolute Magnitudes Estimated by Means of Metallicity and Age

We applied the procedure presented in Section 3.2 to the same clusters, i.e. M3, M53, M71, NGC 188, NGC 6366, IC 4499, and Ter 7, and estimated two sets of absolute magnitudes for the colour indices $(B - V)_0 = 1.05, 1.10, 1.15, 1.20, 1.25, 1.30, 1.35$. We used the coefficients c_i and d_i in Table 8 and Table 9 for the two sets of absolute magnitudes. The ages and metallicities of the clusters used in the corresponding equations are

Table 11: Fiducial giant sequences for the Galactic clusters used in the application of the procedure.

$B - V$	V	$(B - V)_0$	V_0	$B - V$	V	$(B - V)_0$	V_0	$B - V$	V	$(B - V)_0$	V_0
M3				M71				IC 4499			
1.550	12.62	1.540	12.59	1.720	12.50	1.440	11.63	1.440	15.00	1.210	14.29
1.500	12.70	1.490	12.67	1.550	13.00	1.270	12.13	1.377	15.20	1.147	14.49
1.400	12.90	1.390	12.87	1.420	13.50	1.140	12.63	1.318	15.40	1.088	14.69
1.300	13.14	1.290	13.11	1.305	14.00	1.025	13.13	1.264	15.60	1.034	14.89
1.200	13.40	1.190	13.37	1.210	14.50	0.930	13.63	1.213	15.80	0.983	15.09
1.100	13.66	1.090	13.63	1.150	15.00	0.870	14.13	1.166	16.00	0.936	15.29
1.000	14.04	0.990	14.01	1.100	15.50	0.820	14.63	1.124	16.20	0.894	15.49
0.950	14.25	0.940	14.22	1.075	16.00	0.795	15.13	1.085	16.40	0.855	15.69
0.900	14.65	0.890	14.62	1.060	16.50	0.780	15.63	1.051	16.60	0.821	15.89
0.860	15.00	0.850	14.97	1.040	17.00	0.760	16.13	1.020	16.80	0.790	16.09
0.820	15.50	0.810	15.47	NGC 188				0.994	17.00	0.764	16.29
M53				1.387	12.00	1.292	11.71	0.971	17.20	0.741	16.49
1.476	13.83	1.456	13.77	1.305	12.54	1.210	12.25	0.953	17.40	0.723	16.69
1.316	14.05	1.296	13.99	1.233	13.00	1.138	12.71	0.938	17.60	0.708	16.89
1.226	14.29	1.206	14.23	1.162	13.50	1.067	13.21	0.910	18.00	0.680	17.29
1.126	14.49	1.106	14.43	1.112	14.00	1.017	13.71	0.896	18.20	0.666	17.49
1.072	14.72	1.052	14.66	1.091	14.25	0.996	13.96	0.887	18.40	0.657	17.69
1.023	14.88	1.003	14.82	1.060	14.75	0.965	14.46	0.878	18.60	0.648	17.89
0.971	15.07	0.951	15.01	1.028	15.00	0.933	14.71	0.871	18.80	0.641	18.09
0.949	15.30	0.929	15.24	NGC 6366				0.863	19.00	0.633	18.29
0.911	15.50	0.891	15.44	2.100	13.38	1.400	11.21	0.858	19.20	0.628	18.49
0.882	15.68	0.862	15.62	2.010	13.42	1.310	11.25	0.853	19.40	0.623	18.69
0.856	15.89	0.836	15.83	1.970	13.52	1.270	11.35	0.848	19.60	0.618	18.89
0.823	16.10	0.803	16.04	1.930	13.64	1.230	11.47	0.844	19.80	0.614	19.09
0.802	16.29	0.782	16.23	1.840	13.97	1.140	11.80	Terzan7			
0.787	16.50	0.767	16.44	1.750	14.35	1.050	12.18	1.770	15.05	1.700	14.83
0.772	16.70	0.752	16.64	1.690	14.66	0.990	12.49	1.420	15.55	1.350	15.33
0.748	16.90	0.728	16.84	1.650	14.97	0.950	12.80	1.140	16.75	1.070	16.53
0.735	17.08	0.715	17.02	1.620	15.23	0.920	13.06	0.960	18.25	0.890	18.03
0.717	17.31	0.697	17.25	1.600	15.40	0.900	13.23	0.860	19.25	0.790	19.03
0.700	17.50	0.680	17.44	1.570	15.55	0.870	13.38	0.840	19.75	0.770	19.53
0.686	17.68	0.666	17.62	1.560	15.76	0.860	13.59	0.810	20.22	0.740	20.00
0.675	17.91	0.655	17.85	1.540	16.00	0.840	13.83	—	—	—	—
0.660	18.09	0.640	18.03	1.530	16.29	0.830	14.12	—	—	—	—
0.654	18.30	0.634	18.24	1.520	16.42	0.820	14.25	—	—	—	—
0.643	18.50	0.623	18.44	1.500	16.67	0.800	14.50	—	—	—	—
0.626	18.69	0.606	18.63	1.480	17.00	0.780	14.83	—	—	—	—
0.620	18.91	0.600	18.85	1.470	17.35	0.770	15.18	—	—	—	—
0.612	19.09	0.592	19.03	1.460	17.51	0.760	15.34	—	—	—	—
0.597	19.30	0.577	19.24	1.450	17.66	0.750	15.49	—	—	—	—
—	—	—	—	1.440	18.02	0.740	15.85	—	—	—	—

Table 12: $(M_V)_*$ absolute magnitudes and the residuals estimated by the procedure explained in our work. The columns give: (1) $(B-V)_0$ colour index, (2) M_V , absolute magnitude for the cluster estimated by its colour magnitude diagram, (3) $(M_V)_{M5}$, absolute magnitude corresponding to the cluster M5, (4) $\Delta[Fe/H]$, metallicity offset from the metallicity of cluster M5, (5) ΔM , absolute magnitude offset from the fiducial giant sequence of cluster M5, (6) $(M_V)_*$, the absolute magnitude estimated by the procedure, (7) absolute magnitude residuals: $M_V - (M_V)_*$.

1	2	3	4	5	6	7	1	2	3	4	5	6	7
$(B-V)_0$	M_V	$(M_V)_{M5}$	$\Delta[Fe/H]$	ΔM	$(M_V)_*$	$(2)-(6)$	$(B-V)_0$	M_V	$(M_V)_{M5}$	$\Delta[Fe/H]$	ΔM	$(M_V)_*$	$(2)-(6)$
M3							M53 (cont.)						
0.85	-0.07	0.45	-0.33	-0.76	-0.31	0.24	0.97	-1.28	-0.41	-0.82	-1.21	-1.62	0.34
0.90	-0.52	0.05	-0.33	-0.71	-0.66	0.14	1.00	-1.42	-0.58	-0.82	-1.17	-1.75	0.33
0.95	-0.85	-0.29	-0.33	-0.67	-0.96	0.10	1.02	-1.50	-0.69	-0.82	-1.15	-1.84	0.34
1.00	-1.10	-0.58	-0.33	-0.63	-1.21	0.11	1.05	-1.61	-0.84	-0.82	-0.88	-1.72	0.10
1.05	-1.28	-0.84	-0.33	-0.28	-1.11	-0.17	1.10	-1.78	-1.07	-0.82	-0.86	-1.93	0.16
1.10	-1.44	-1.07	-0.33	-0.28	-1.35	-0.09	1.12	-1.84	-1.16	-0.82	-0.87	-2.03	0.19
1.15	-1.58	-1.29	-0.33	-0.31	-1.60	0.02	1.15	-1.92	-1.29	-0.82	-0.87	-2.15	0.23
1.20	-1.71	-1.49	-0.33	-0.33	-1.82	0.11	1.17	-1.97	-1.37	-0.82	-0.87	-2.23	0.26
1.25	-1.84	-1.67	-0.33	-0.33	-1.99	0.16	1.20	-2.04	-1.49	-0.82	-0.86	-2.34	0.30
1.30	-1.96	-1.83	-0.33	-0.31	-2.13	0.17	1.22	-2.09	-1.56	-0.82	-0.85	-2.41	0.32
1.35	-2.09	-1.96	-0.33	-0.28	-2.24	0.16	1.25	-2.16	-1.67	-0.82	-0.83	-2.50	0.34
1.40	-2.20	-2.07	-0.33	-0.54	-2.61	0.40	1.27	-2.20	-1.73	-0.82	-0.82	-2.56	0.36
1.45	-2.31	-2.16	-0.33	-0.16	-2.33	0.02	1.30	-2.26	-1.83	-0.82	-0.81	-2.64	0.38
1.50	-2.40	-2.24	-0.33	-0.11	-2.35	-0.05	1.32	-2.30	-1.88	-0.82	-0.80	-2.69	0.39
M71							1.35	-2.35	-1.96	-0.82	-0.78	-2.74	0.39
0.80	2.20	0.96	0.39	1.59	2.54	-0.34	1.37	-2.39	-2.01	-0.82	-0.76	-2.76	0.38
0.85	1.40	0.45	0.39	1.27	1.72	-0.32	Ter7						
0.90	0.93	0.05	0.39	1.18	1.22	-0.29	0.75	3.01	1.61	0.30	1.54	3.15	-0.15
0.95	0.63	-0.29	0.39	1.12	0.83	-0.19	0.77	2.69	1.33	0.30	1.37	2.70	-0.01
1.00	0.39	-0.58	0.39	1.07	0.49	-0.10	0.80	2.25	0.96	0.30	1.18	2.13	0.11
1.05	0.15	-0.84	0.39	0.63	-0.20	0.35	0.82	1.98	0.74	0.30	1.09	1.83	0.15
1.10	-0.10	-1.07	0.39	0.62	-0.45	0.34	0.85	1.60	0.45	0.30	1.00	1.45	0.15
1.15	-0.35	-1.29	0.39	0.66	-0.63	0.28	0.90	1.06	0.05	0.30	0.91	0.96	0.11
1.20	-0.57	-1.49	0.39	0.67	-0.81	0.24	0.92	0.87	-0.10	0.30	0.89	0.80	0.08
1.25	-0.74	-1.67	0.39	0.67	-1.00	0.26	0.95	0.61	-0.29	0.30	0.87	0.58	0.03
1.30	-0.85	-1.83	0.39	0.66	-1.17	0.31	0.97	0.45	-0.41	0.30	0.85	0.44	0.00
1.35	-0.94	-1.96	0.39	0.64	-1.32	0.38	1.00	0.22	-0.58	0.30	0.84	0.26	-0.04
1.40	-1.08	-2.07	0.39	0.74	-1.34	0.26	1.02	0.08	-0.69	0.30	0.82	0.14	-0.06
1.45	-1.41	-2.16	0.39	0.90	-1.27	-0.14	1.05	-0.11	-0.84	0.30	0.48	-0.35	0.24
NGC188							1.10	-0.40	-1.07	0.30	0.48	-0.59	0.19
1.00	2.79	-0.58	1.17	2.71	2.13	0.66	1.12	-0.51	-1.16	0.30	0.49	-0.67	0.16
1.02	2.56	-0.69	1.17	2.61	1.92	0.63	1.15	-0.66	-1.29	0.30	0.51	-0.78	0.12
1.05	2.23	-0.84	1.17	2.92	2.09	0.14	1.17	-0.75	-1.37	0.30	0.51	-0.86	0.10
1.07	2.03	-0.93	1.17	2.87	1.93	0.10	1.20	-0.89	-1.49	0.30	0.52	-0.97	0.08
1.10	1.77	-1.07	1.17	2.77	1.70	0.07	1.22	-0.97	-1.56	0.30	0.52	-1.04	0.07
1.12	1.62	-1.16	1.17	2.72	1.56	0.07	1.25	-1.10	-1.67	0.30	0.52	-1.15	0.05
1.15	1.43	-1.29	1.17	2.65	1.36	0.07	1.27	-1.18	-1.73	0.30	0.52	-1.22	0.04
1.17	1.31	-1.37	1.17	2.61	1.24	0.07	1.30	-1.29	-1.83	0.30	0.51	-1.31	0.02
1.20	1.16	-1.49	1.17	2.56	1.07	0.08	1.32	-1.36	-1.88	0.30	0.51	-1.37	0.01
1.22	1.05	-1.56	1.17	2.53	0.97	0.08	1.35	-1.47	-1.96	0.30	0.50	-1.46	-0.01
1.25	0.87	-1.67	1.17	2.48	0.81	0.06	1.37	-1.53	-2.01	0.30	0.50	-1.51	-0.02
1.27	0.73	-1.73	1.17	2.44	0.71	0.02	1.40	-1.63	-2.07	0.30	0.62	-1.45	-0.17
1.30	0.44	-1.83	1.17	2.37	0.55	-0.11	1.42	-1.68	-2.11	0.30	0.62	-1.49	-0.19
IC4499							1.45	-1.77	-2.16	0.30	0.66	-1.50	-0.26
0.80	-0.34	0.96	-0.36	-1.03	-0.07	-0.28	NGC 6366						
0.82	-0.46	0.74	-0.36	-0.96	-0.22	-0.24	0.85	1.50	0.45	0.50	1.58	2.04	-0.54
0.85	-0.62	0.45	-0.36	-0.83	-0.38	-0.25	0.90	0.94	0.05	0.50	1.50	1.54	-0.61
0.90	-0.88	0.05	-0.36	-0.77	-0.72	-0.16	0.92	0.76	-0.10	0.50	1.46	1.37	-0.61
0.92	-0.99	-0.10	-0.36	-0.75	-0.84	-0.14	0.95	0.52	-0.29	0.50	1.42	1.13	-0.61
0.95	-1.14	-0.29	-0.36	-0.72	-1.01	-0.13	0.97	0.38	-0.41	0.50	1.39	0.98	-0.60
0.97	-1.24	-0.41	-0.36	-0.71	-1.12	-0.12	1.00	0.20	-0.58	0.50	1.35	0.77	-0.57
1.00	-1.37	-0.58	-0.36	-0.69	-1.27	-0.10	1.02	0.09	-0.69	0.50	1.32	0.64	-0.55
1.02	-1.45	-0.69	-0.36	-0.67	-1.36	-0.09	1.05	-0.06	-0.84	0.50	0.84	0.00	-0.07
1.05	-1.56	-0.84	-0.36	-0.31	-1.14	-0.41	1.10	-0.29	-1.07	0.50	0.82	-0.25	-0.04
1.07	-1.62	-0.93	-0.36	-0.30	-1.23	-0.39	1.12	-0.37	-1.16	0.50	0.84	-0.32	-0.05
1.10	-1.69	-1.07	-0.36	-0.31	-1.38	-0.31	1.15	-0.50	-1.29	0.50	0.86	-0.43	-0.07
1.12	-1.74	-1.16	-0.36	-0.32	-1.48	-0.26	1.17	-0.57	-1.37	0.50	0.87	-0.50	-0.07
1.15	-1.81	-1.29	-0.36	-0.35	-1.63	-0.18	1.20	-0.68	-1.49	0.50	0.88	-0.61	-0.07
1.17	-1.87	-1.37	-0.36	-0.36	-1.73	-0.14	1.22	-0.75	-1.56	0.50	0.88	-0.68	-0.07
1.20	-2.00	-1.49	-0.36	-0.36	-1.85	-0.14	1.25	-0.85	-1.67	0.50	0.87	-0.80	-0.05
1.22	-2.12	-1.56	-0.36	-0.37	-1.93	-0.20	1.27	-0.91	-1.73	0.50	0.86	-0.87	-0.04
M53							1.30	-0.98	-1.83	0.50	0.85	-0.98	0.00
0.85	-0.56	0.45	-0.82	-1.53	-1.08	0.52	1.32	-1.02	-1.88	0.50	0.84	-1.04	0.03
0.90	-0.90	0.05	-0.82	-1.36	-1.31	0.41	1.35	-1.05	-1.96	0.50	0.82	-1.14	0.09
0.92	-1.02	-0.10	-0.82	-1.31	-1.40	0.38	1.37	-1.06	-2.01	0.50	0.81	-1.20	0.14
0.95	-1.18	-0.29	-0.82	-1.24	-1.53	0.35	1.40	-1.05	-2.07	0.50	0.87	-1.20	0.15

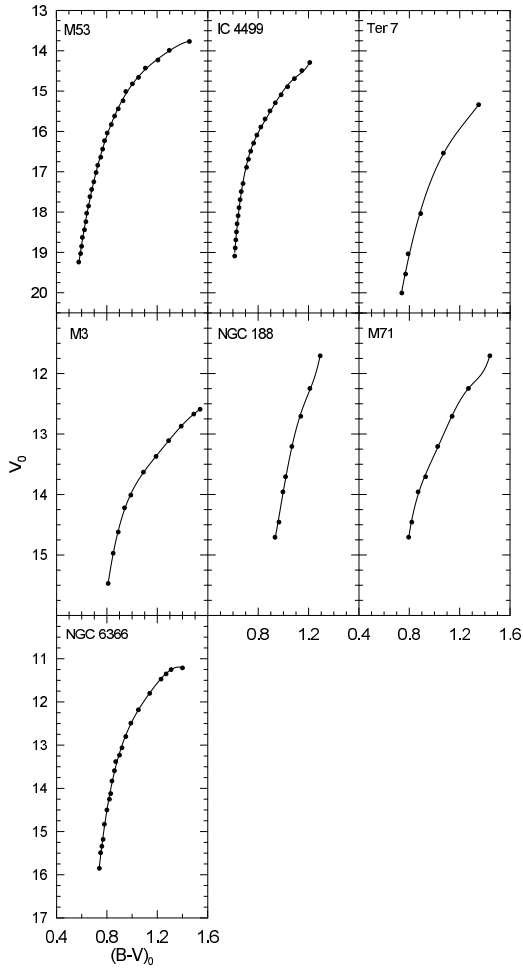


Figure 5: $V_0 \times (B - V)_0$ colour-apparent magnitude diagrams for the Galactic clusters used for the application of the procedure.

taken from Table 7 and Table 10. The results are given in Table 14 and Table 15.

We compared the absolute magnitude residuals evaluated via three procedures for the colour indices $(B - V)_0 = 1.05, 1.10, 1.15, 1.20, 1.25, 1.30, 1.35$ which are given in Tables 12, 14 and 15, in order to choose the most advantage one and to test the effect of the age in absolute magnitude estimation of the red giants. The best statistic is the couple of their mean and standard deviation for this purpose. Table 16 shows that the three procedures provide absolute magnitudes agreeable with the ones appeared in the literature. However, the range of the residuals for the absolute magnitudes evaluated by the procedures which involve age as a term are larger. That is, the procedure where the absolute magnitude is fitted to a third degree polynomial of the metallicity has an advantage respect to the others two. Hence, the procedures with large range of

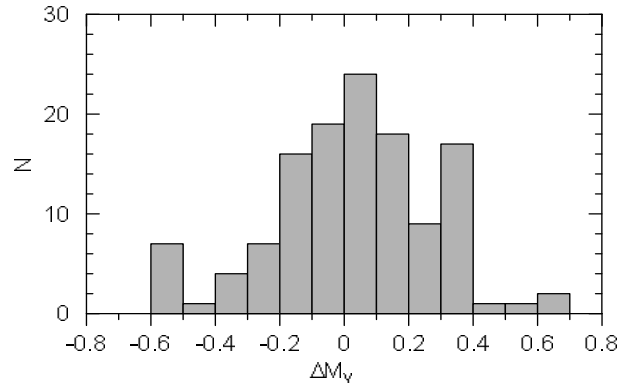


Figure 6: Histogram of the residuals.

Table 13: Distribution of residuals. N denotes the number of stars.

ΔM -interval	$\langle \Delta M \rangle$	N
$(-0.6, -0.5]$	-0.58	7
$(-0.5, -0.4]$	-0.41	1
$(-0.4, -0.3]$	-0.34	4
$(-0.3, -0.2]$	-0.25	7
$(-0.2, -0.1]$	-0.15	16
$(-0.1, 0.0]$	-0.05	19
$(0.0, 0.1]$	0.06	24
$(0.1, 0.2]$	0.15	18
$(0.2, 0.3]$	0.26	9
$(0.3, 0.4]$	0.36	17
$(0.4, 0.5]$	0.41	1
$(0.5, 0.6]$	0.52	1
$(0.6, 0.7]$	0.65	2

absolute magnitude residuals have not been extended to the other $(B - V)_0$ colour indices.

The absolute magnitudes on the RGB at a given colour and metallicity do not change linearly or quadratically with age, as implied by the form of Eqs. (4) and (5). Instead, the absolute magnitude gets rapidly fainter for young (and so massive) stars with a certain $B - V$ and $[Fe/H]$, but shows virtually the same absolute magnitude for all old stars, i.e. $t > 6$ Gyr.

4 Summary and Discussion

We presented an absolute magnitude calibration for red giants based on the colour-magnitude diagrams of six Galactic clusters with different metallicities, i.e. M92, M13, M5, 47 Tuc, M67, and NGC 6791. We combined the calibrations be-

Table 14: Absolute magnitudes (second column) and residuals (fourth column) estimated by the procedure explained in Section 3.2. The coefficients c_i ($i = 0, 1, 2, 3, 4, 5$) are taken from Table 8. The absolute magnitude M_{cl} (taken from Table 12) indicates the absolute magnitude estimated by the colour magnitude diagram of the corresponding cluster.

$(B - V)_0$	Cluster	M_{ev}	M_{cl}	ΔM
1.05	M3	-1.38	-1.28	0.10
1.05	M53	-1.77	-1.61	0.16
1.05	M71	0.25	0.15	-0.10
1.05	NGC 188	2.53	2.23	-0.30
1.05	NGC 6366	0.28	-0.06	-0.34
1.05	IC 4499	-1.42	-1.56	-0.14
1.05	Ter 7	-0.23	-0.11	0.12
1.10	M3	-1.61	-1.44	0.17
1.10	M53	-2.00	-1.78	0.22
1.10	M71	-0.05	-0.10	-0.05
1.10	NGC 188	2.13	1.77	-0.36
1.10	NGC 6366	-0.16	-0.29	-0.13
1.10	IC 4499	-1.96	-1.69	0.27
1.10	Ter 7	-0.69	-0.40	0.29
1.15	M3	-1.71	-1.58	0.13
1.15	M53	-2.06	-1.92	0.14
1.15	M71	-0.25	-0.35	-0.10
1.15	NGC 188	1.86	1.43	-0.43
1.15	NGC 6366	-0.37	-0.50	-0.13
1.15	IC 4499	-2.07	-1.81	0.26
1.15	Ter 7	-0.87	-0.66	0.21
1.20	M3	-1.74	-1.71	0.03
1.20	M53	-2.03	-2.04	-0.01
1.20	M71	-0.39	-0.57	-0.18
1.20	NGC 188	1.62	1.16	-0.46
1.20	NGC 6366	-0.55	-0.68	-0.13
1.20	IC 4499	-2.13	-2.00	0.13
1.20	Ter 7	-1.24	-0.89	0.35
1.25	M3	-2.81	-1.84	0.97
1.25	M53	-3.26	-2.16	1.10
1.25	M71	-1.22	-0.74	0.48
1.25	NGC 188	1.18	0.87	-0.31
1.25	NGC 6366	-1.21	-0.85	0.36
1.25	Ter 7	-2.02	-1.10	0.92
1.30	M3	-1.92	-1.96	-0.04
1.30	M53	-2.17	-2.26	-0.09
1.30	M71	-0.65	-0.85	-0.20
1.30	NGC 188	1.25	0.44	-0.80
1.30	NGC 6366	-0.89	-0.98	-0.09
1.30	Ter 7	-1.59	-1.29	0.30
1.35	M3	-1.94	-2.09	-0.15
1.35	M53	-2.16	-2.35	-0.19
1.35	M71	-0.72	-0.94	-0.22
1.35	NGC 6366	-1.01	-1.05	-0.04
1.35	Ter 7	-1.71	-1.47	0.24

Table 15: Absolute magnitudes (second column) and residuals (fourth column) estimated by the procedure explained in Section 3.2. The coefficients d_i ($i = 0, 1, 2, 3, 4$) are taken from Table 9. The absolute magnitude M_{cl} (taken from Table 12) indicates the absolute magnitude estimated by the colour magnitude diagram of the corresponding cluster.

$(B - V)_0$	Cluster	M_{ev}	M_{cl}	ΔM
1.05	M3	-1.47	-1.28	0.19
1.05	M53	-1.96	-1.61	0.35
1.05	M71	0.27	0.15	-0.12
1.05	NGC 6366	0.18	-0.06	-0.24
1.05	IC 4499	-1.55	-1.56	-0.01
1.05	Ter 7	-0.31	-0.11	0.20
1.05	NGC 188	2.07	2.23	0.16
1.10	M3	-1.67	-1.44	0.23
1.10	M53	-2.15	-1.78	0.37
1.10	M71	-0.02	-0.10	-0.08
1.10	NGC 6366	-0.10	-0.29	-0.19
1.10	IC 4499	-1.76	-1.69	0.07
1.10	Ter 7	-0.56	-0.40	0.16
1.10	NGC 188	1.69	1.77	0.08
1.15	M3	-1.86	-1.58	0.28
1.15	M53	-2.33	-1.92	0.41
1.15	M71	-0.28	-0.35	-0.07
1.15	NGC 6366	-0.35	-0.50	-0.15
1.15	IC 4499	-1.95	-1.81	0.14
1.15	Ter 7	-0.80	-0.66	0.14
1.15	NGC 188	1.38	1.43	0.05
1.20	M3	-2.04	-1.71	0.33
1.20	M53	-2.48	-2.04	0.44
1.20	M71	-0.51	-0.57	-0.06
1.20	NGC 6366	-0.57	-0.68	-0.11
1.20	IC 4499	-2.13	-2.00	0.13
1.20	Ter 7	-1.02	-0.89	0.13
1.20	NGC 188	1.12	1.16	0.04
1.25	M3	-2.20	-1.84	0.36
1.25	M53	-2.63	-2.16	0.47
1.25	M71	-0.72	-0.74	-0.02
1.25	NGC 6366	-0.78	-0.85	-0.07
1.25	Ter 7	-1.21	-1.10	0.11
1.25	NGC 188	0.88	0.87	-0.01
1.30	M3	-2.35	-1.96	0.39
1.30	M53	-2.77	-2.26	0.51
1.30	M71	-0.88	-0.85	0.03
1.30	NGC 6366	-0.98	-0.98	0.00
1.30	Ter 7	-1.40	-1.29	0.11
1.30	NGC 188	0.66	0.44	-0.22
1.35	M3	-2.47	-2.09	0.38
1.35	M53	-2.88	-2.35	0.53
1.35	M71	-1.02	-0.94	0.08
1.35	NGC 6366	-1.15	-1.05	0.10
1.35	Ter 7	-1.55	-1.47	0.08

Table 16: Mean ($\langle \Delta M \rangle$) and standard deviation (σ) for the absolute magnitude residuals for three procedures. (1), (2), and (3) in the first column refer to the procedures given in Sections 3.3.1, 3.3.2 with coefficients c_i , and Section 3.3.2 but with coefficients d_i

Procedure	$\langle \Delta M \rangle$	σ
1	0.12	0.20
2	0.04	0.36
3	0.13	0.21

tween V_0 and $(B-V)_0$ for each cluster with their true distance modulus and evaluated a set of absolute magnitudes for the $(B-V)_0$ range of each clusters. We adopted the V_0 , $(B-V)_0$ calibration of the cluster M5 which is defined in the interval $0.75 \leq (B-V)_0 \leq 1.50$ mag as the standard colour magnitude diagram and evaluated the ΔM offsets from the fiducial red giant sequence of the cluster M5. We, then combined ΔM with the corresponding $\Delta[Fe/H]$ offsets and obtained the required calibration.

We applied the procedure to another set of Galactic cluster, i.e. M3, M53, M71, NGC 188, NGC 6366, IC 4499, and Ter 7. The reason of this choice is that a cluster provides absolute magnitude for comparison with the ones estimated by means of our procedure. We used the calibration in Eq. (3) and evaluated a set of ΔM offsets for each cluster in their $(B-V)_0$ range. We, then added them to the corresponding absolute magnitudes derived for the standard cluster M5 and obtained the required absolute magnitudes. We compared the absolute magnitudes estimated by this procedure with those evaluated via combination of the fiducial V_0 , $(B-V)_0$ sequence and the true distance modulus for each cluster. 91% of the differences between two sets of absolute magnitudes (the residuals) lie in the range $(-0.4, +0.4)$. The mean and the standard deviation of the residuals are 0.05 and 0.19 mag. The residuals cited in this study are at the level of the ones appeared in the literature. We quote two works as example to confirm our argument, i.e. Laird, Carney & Latham (1988) and Karaali et al. (2003).

Comparison of our work with the one of Hog & Flynn (1998) shows that there is an improvement on our results with respect to theirs. Hog & Flynn (1998) fitted the absolute magnitudes of 581 bright K giants in terms of two colours defined in the DDO intermediate band photometry (McClure 1976), i.e. C4245 and C4548, by a quadratic polynomial. Then, they applied two small corrections to obtain more accurate absolute magnitudes. The range of the residuals of the final absolute magnitudes with respect to the *Hipparcos* absolute magnitudes is $[-1, +1]$. They give an accuracy of 0.35

mag which confirm the advantage of our results. We quote also the work of Ljunggren & Oja (1966).

Although age plays an important role in the trend of the fiducial sequence of the RGB, we have not used it as a parameter in this calibration of the absolute magnitude. Another problem may originate from the Red Clump (RC) stars. These stars lie very close to the RGB but they present a completely different group of stars. Table 13 and Fig. 6 summarize how reliable are our absolute magnitudes. If age and possibly the mix with RC stars would affect our results this should show up. Additionally, we should add that the fiducial sequences used in our study were properly selected as RGB. However, the researches should identify and exclude the RC stars when they apply our calibrations to the field stars.

Despite the considerations stated in the preceding paragraph, we fitted the absolute magnitude to metallicity and age for a limited sub-sample of $(B-V)_0$ colour, i.e. 1.05, 1.10, 1.15, 1.20, 1.25, 1.30, 1.35, and compared the residuals evaluated by this procedure with the corresponding ones evaluated by means of the former procedure. The results in Table 16 confirm our argument. That is, the procedure where the absolute magnitude fitted to a third degree polynomial of (only) the metallicity provides more reliable absolute magnitudes than the procedure which involves the age as a parameter.

The colour magnitude diagrams displayed in Fig. 2 are smooth and confirm the dependence of the absolute magnitude calibration in Eq. (3) on colour and metallicity. The absolute magnitudes of a cluster with lower metallicity are brighter for given a colour. This argument was used as a tool to prefer the iron abundance $[Fe/H] = -1.17$ to -1.40 dex for the cluster M5, where these values were proposed by Sandquist et al. (1996), and Zinn & West (1984), respectively. The colour magnitude diagram of M5 is about 0.5 mag fainter than the absolute magnitude of M13, for a given colour. Hence, the metallicities of these clusters should be different. As the iron abundance of M13 appeared in the literature is $[Fe/H] = -1.41$ dex (Gratton et al. 1997), the one of M5 should be different than this value.

One requires accurate metallicity and interstellar extinction determination for the application of the procedure to the field stars. The absolute magnitude could be calibrated as a function of ultraviolet excess, instead of metallicity. However, accurate ultraviolet magnitudes can not be provided easily. Whereas, metallicity can be derived by different methods, such as by means of atmospheric parameters of a star, a procedure which is applied rather extensively in large surveys such as RAdial Velocity Experiment (RAVE; Steinmetz et al. 2006). In such cases, one needs to transform the calibration from BV to the system in question. The clusters considered

in our paper are relatively old, $t \geq 4$ Gyr. For such stars the age is a secondary parameter and does not influence much the position of the RGB sequence. However, the field stars can be much younger. We should remind that the derived relations are applicable only to stars older than 4 Gyr.

Acknowledgments

We thank to the anonymous reviewer for his/her comments and suggestions. This research has made use of NASA's Astrophysics Data System and the SIMBAD database, operated at CDS, Strasbourg, France.

References

- Alonso, M. V., Salaris, M., Martinez-Roger, C., Straniero, O., Arribas, S. 1997, *A&A*, 323, 374
- Breddels, M. A., et al. 2010, *A&A*, 511A, 90
- Buonanno, R., Corsi, C. E., Pulone, L., Pecci, F. F., Richer, H. B., Fahlman, G. C. 1995, *AJ*, 109, 663
- Chen, B., et al. 2001, *ApJ*, 553, 184
- Gratton, R. G., Fusi Pecci, F., Carretta, E., Clementini, G., Corsi, C. E., Lattanzi, M. 1997, *ApJ*, 491, 749
- Harris, W. E. 1996, *AJ*, 112, 1487
- Harris, W. E. 2010 arXiv:1012.3224
- Hesser, J. E., Harris, W. E., Vandenberg, D. A., Allwright, J. W. B., Shott, P., Stetson, P. B. 1987, *PASP*, 99, 739
- Hodder, P. J. C., Nemec, J. M., Richer, H. B., Fahlman, G. G. 1992, *AJ*, 103, 460
- Hog, E., Flynn, C. 1998, *MNRAS*, 294, 28
- Karaali, S., Karataş, Y., Bilir, S., Ak, S. G., Hamzaoglu, E. 2003, *PASA*, 20, 270
- Laird, J. B., Carney, B. W., Latham, D. W. 1988, *AJ*, 96, 1908
- Ljunggren, B., Oja, T. 1966, *IAUS*, 24, 317
- Marigo, P., Girardi, L., Bressan, A., Groenewegen, M. A. T., Silva, L., Granato, G. L. 2008, *A&A*, 482, 883
- McClure, R. D. 1976, *AJ*, 81, 182
- Meibom, S., Grundahl, F., Clausen, J. V., Mathieu, R. D., Frandsen, S., Pigulski, A., Narwid, A., Steslicki, M., Lefever, K. 2009, *AJ*, 137, 5086
- Nissen, P. E., Schuster, W. J. 1991, *A&A*, 251, 457
- Percival, S. M., Salaris, M., van Wyk, F., Kilkeny, D. 2002, *ApJ*, 573, 174
- Perryman, M. A. C., et al. 1997, *A&A*, 323, L49, (ESA, 1997)
- Phleps, S., Meisenheimer, K., Fuchs, B., Wolf, C. 2000, *A&A*, 356, 108
- Rey, S.-C., Lee, Y.-W., Byun, Y.-I., Chun, M.-S. 1998, *AJ*, 116, 1775
- Salaris, M., Weiss, A. 2002, *A&A*, 388, 492
- Sandage, A. 1970, *ApJ*, 162, 841
- Sandage, A., Lubin, L. M., Vandenberg, D. A. 2003, *PASP*, 115, 1187
- Sandquist, E. L., Bolte, M., Stetson, P. B., Hesser, J. E. 1996, *ApJ*, 470, 910
- Santos, J. F. C. Jr., Piatti, A. E. 2004, *A&A*, 428, 79
- Sarajedini, A. 1993, *AJ*, 105, 2172
- Siegel, M. H., Majewski, S. R., Reid, I. N., Thompson, I. B. 2002, *ApJ*, 578, 151
- Steinmetz, M., et al. 2006, *AJ*, 132, 1645
- Stetson, P. B., Harris, W. E. 1988, *AJ*, 96, 909
- Vandenberg, D. A., Bergbusch, P. A., Dowler, P. D. 2006, *ApJS*, 162, 375
- Zinn, R., West, M. J. 1984, *ApJS*, 55, 45
- Zwitter, T., et al. 2010, *A&A*, 522A, 54